

# Spatial Separation of Large Earthquakes, Aftershocks, and Background Seismicity: Analysis of Interseismic and Coseismic Seismicity Patterns in Southern California

EGILL HAUSSON<sup>1</sup>

**Abstract**—We associate waveform-relocated background seismicity and aftershocks with the 3-D shapes of late Quaternary fault zones in southern California. Major earthquakes that can slip more than several meters, aftershocks, and near-fault background seismicity mostly rupture different surfaces within these fault zones. Major earthquakes rupture along the mapped traces of the late Quaternary faults, called the principal slip zones (PSZs). Aftershocks occur either on or in the immediate vicinity of the PSZs, typically within zones that are  $\pm 2$ -km wide. In contrast, the near-fault background seismicity is mostly accommodated on a secondary heterogeneous network of small slip surfaces, and forms spatially decaying distributions extending out to distances of  $\pm 10$  km from the PSZs. We call the regions where the enhanced rate of background seismicity occurs, the seismic damage zones. One possible explanation for the presence of the seismic damage zones and associated seismicity is that the damage develops as faults accommodate bends and geometrical irregularities in the PSZs. The seismic damage zones mature and reach their finite width early in the history of a fault, during the first few kilometers of cumulative offset. Alternatively, the similarity in width of seismic damage zones suggests that most fault zones are of almost equal strength, although the amount of cumulative offset varies widely. It may also depend on the strength of the fault zone, the time since the last major earthquake as well as other parameters. In addition, the seismic productivity appears to be influenced by the crustal structure and heat flow, with more extensive fault networks in regions of thin crust and high heat flow.

**Key words:** Seismicity, California, faults, aftershocks, interseismic seismicity, fault damage zones, San Andreas fault system, evolution of fault zones, earthquake interaction.

## 1. Introduction

We analyze the Southern California seismicity located in the vicinity of late Quaternary faults to

answer the question whether large earthquakes, aftershocks, and background seismicity occur within the same parts of fault zones that are often several kilometers wide. Establishing this spatial relationship is the first step towards understanding the difference in source physics between large and small earthquakes.

In the 1920s Dr. Harry Wood of the Carnegie Institute in Pasadena (today known as the Caltech Seismological Laboratory) proposed that a seismic network should be installed in southern California (WOOD, 1916). He argued that recording the more frequent small earthquakes would help us understand future large damaging earthquakes. The Southern California Seismic Network (SCSN), now a joint project of Caltech and USGS, has been in operation since then and recorded more than 400,000 both small and large earthquakes. During the same time period, geologists have collected data on late Quaternary faults in southern California (e.g., FRANKEL *et al.*, 2002). We synthesize both data sets in an attempt to answer some of the questions regarding how seismicity and faults are related as proposed by Dr. Wood in 1916.

We analyze the southern California earthquake catalog from 1981 to 2005, and the data set of fault segments or principal slip zones (PSZs) of the Southern California Earthquake Center Community Fault Model (SCEC/CFM) (PLESCH *et al.*, 2007). The PSZs accommodate the major earthquakes and thus could have different material properties as well as strength than the adjacent crust. Commonly, the thickness of faults is considered to be smaller than 10 m, with maximum shear on the PSZ occurring on the outer surfaces of fault cores (CHAMBON *et al.*,

---

<sup>1</sup> Seismological Laboratory, Division of Geological and Planetary Sciences, California Institute of Technology, Pasadena, CA 91125, USA. E-mail: Hauksson@gps.caltech.edu

2006). The thickness of the principal slip zone is thought to be small or only 1- to 10-mm wide (SIBSON, 2003). Their lengths may extend from 10 to 100 s of kilometers while their depths usually extend to 15 km or as much as 25 km. The relationship between large earthquakes and late Quaternary faults is obvious when a large earthquake ruptures the surface (e.g., SIEH *et al.*, 1993). Because the background seismicity has no surface rupture, we use the location of the hypocenter relative to the fault surface to infer the spatial relationship between the seismicity and the PSZs.

Several recent studies have attempted to associate earthquakes and faults in southern California. Analyzing seismicity around a few strike-slip faults, WESNOSKY (1990) inferred that the background seismicity rate adjacent to late Quaternary faults in southern California was controlled by cumulative fault offset. Focusing on the 1992 Landers aftershocks, LIU *et al.* (2003), studied the relationship of the aftershocks to the main shock PSZs to estimate

the size of the seismic damage zone. They showed that the Landers aftershocks formed a narrow spatial distribution around the PSZ, although only a small fraction of aftershocks seemed to be caused by slip on the PSZ. More recently, WESSON *et al.* (2003) developed a Bayesian technique for associating historical and instrumental seismicity with faults in the San Francisco Bay area, California. WOESSNER and HAUKSSON (2006) used the Bayesian statistics technique to associate the southern California background seismicity to the CFM, and synthesized the overall statistical patterns. They showed that  $\sim 40\%$  of earthquakes occur within 2 km and 60% within 4 km, and found evidence for larger earthquakes being preferentially located closer to the major fault zones.

To identify spatial alignments, we plot the background seismicity in colors as a function of distance from the nearest fault segment (Fig. 1). The bright red to yellow alignments of seismicity such as parts of the San Andreas fault, the San Jacinto fault, the southern Sierra Nevada, and the aftershock zones of

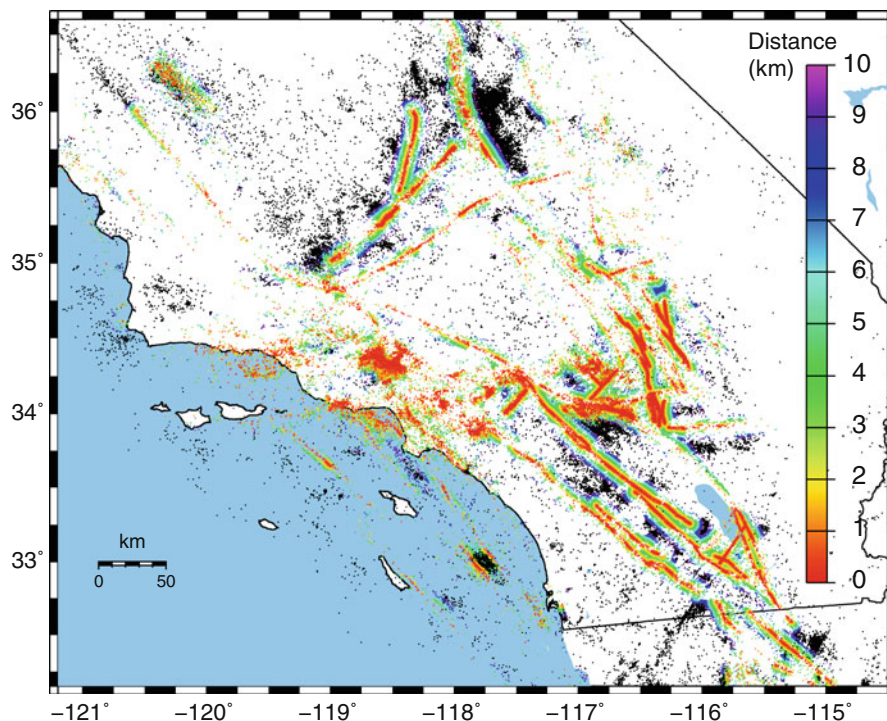


Figure 1

Late Quaternary fault traces are not plotted on this map. Map showing the southern California relocated seismicity from 1981 through 2005. Each epicenter is colored to show the distance from the nearest mapped late Quaternary fault segment (SCEC/CFM), with color bar from 0 to 10 km. Earthquakes in the distance range of 10–20 km are plotted in black. Note how the major faults are illuminated by the adjacent seismicity

the 1992 Landers and 1999 Hector Mine earthquakes, identify where the seismicity is concentrated near PSZs. In contrast, several both high and low slip-rate faults located in the Western Transverse Ranges as well as the Mojave Desert are not surrounded by significant seismicity, illustrating that the relationship between background seismicity and faults is complex.

There are many factors that may influence the seismicity distribution around the PSZ of a fault. The strength of the fault and varying loading of fault zones may affect the width of the seismicity distribution near the PSZs. The geometrical shape and productivity of a seismicity distribution may depend on where within the seismic cycle the fault segment happens to be. For instance, if the fault just had a main shock the seismic damage zone may be dominated by aftershocks. Alternatively, if the fault is late in the seismic cycle it could have returned to normal background seismicity. The age of the fault, initial growth of complexity, and subsequent smoothing of the fault (e.g., SAGY *et al.*, 2007) may influence the seismicity distribution adjacent to the PSZs. Similarly, external effects such as triggering or regional stress release caused by other earthquakes may influence the seismicity. Thus, synthesizing the seismicity with the fault zone properties may provide new understanding of which of these processes are more important than others.

## 2. Earthquake Data

We analyze the earthquake catalog from the Southern California Seismic Network, a joint project of the USGS and Caltech. LIN *et al.* (2007) relocated this catalog to improve the earthquake hypocenters by using absolute travel times and cross-correlation differential travel times as well as double-difference type location techniques. We determined the statistical properties (mean and standard deviation) of the seismicity distributions next to each fault segment using a routine from PRESS *et al.* (1997).

We also analyzed the Southern California Earthquake Center community fault model (SCEC/CFM 3.0), which is a model of fault segments rather than many segments daisy-chained into whole faults

(PLESCH *et al.*, 2007). The SCEC/CFM consists of 162 principal slip zones (PSZ) of late Quaternary faults that are mapped in three dimensions (3-D) (Fig. 2). The SCEC/CFM fault model is based mostly on geological data, although in some instances seismicity data are included. The segmentation is somewhat subjective, for instance, the southern San Andreas fault consists of more than four segments, and the Garlock fault consists of only one segment. Short fault segments are more common than long ones. The three-dimensional (3-D) shapes of principal slip surfaces are defined in the SCEC/CFM representation.

A subset of 75 SCEC/CFM fault segments has measured or assigned slip-rates, which have varying error bars (FRANKEL *et al.*, 2002; S. Perry, written communication, 2007). Because both the locations of the seismic stations and the locations of the fault segments are based on global positioning measurements (GPS), it becomes possible to evaluate their relative positions. A. Plesch (written communication, 2007) provided the Euclidian measurements of distances from each hypocenter to the nearest principal slip surface in the SCEC/CFM.

The uncertainties and biases in the data used in this study could affect the results variously. For instance, the PSZs may be incorrectly mapped at the surface or field data incorrectly digitized. Alternatively, a PSZ could be assigned the wrong dip or could have a more complex shape than can be inferred at the surface. In these cases, the mean of the cluster would be offset and in some cases the distribution could be artificially skewed. The earthquake location mean absolute horizontal and depth errors are  $\sim 0.2$  and  $\sim 0.4$  km, respectively, while the relative errors are a factor of ten smaller (LIN *et al.*, 2007). Thus, in extreme cases, the hypocenters may be mislocated by up to at most 1 km horizontally and 2 km in depth, although this is unlikely. Because the velocity contrasts across faults in southern California are usually small, we do not expect systematic location biases but rather random errors, which will have insignificant effects. If faults are closely spaced, some seismicity may be assigned to one fault rather than the other, which causes minor artificial biases in evaluating the seismicity for individual segments.

To average out some of the uncertainties in the data sets and to analyze how the different faulting and

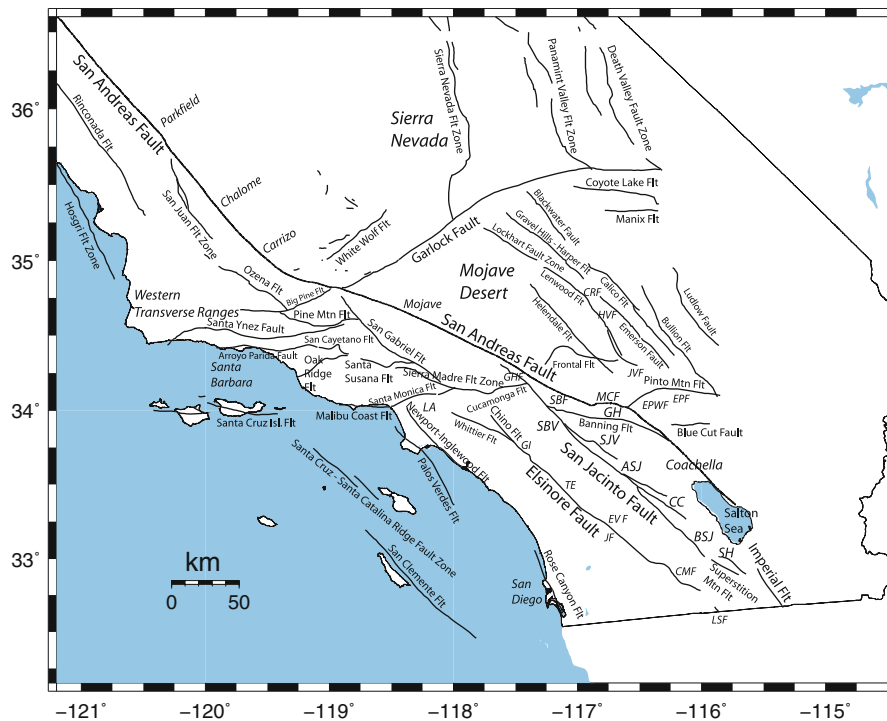


Figure 2

Simplified fault map of southern California based on the JENNINGS (1994) map. *ASJ*—Anza San Jacinto, *BSJ*—Borrego San Jacinto, *CC*—Coyote Creek, *CMF*—Coyote Mountain fault, *CRF*—Camp-Rock fault, *EPF*—Eureka Peak fault, *EPWF*—Eureka Peak West fault, *EVF*—Earthquake Valley fault, *GH*—Garnet Hill, *GHF*—Glen Helen Fault, *GI*—Glenn Ivy, *HVF*—Homestead Valley fault, *JF*—Julian Fault, *JVF*—Johnson Valley fault, *LA*—Los Angeles, *LSF*—Laguna Salada fault, *SBV*—San Bernardino Valley, *SH*—Superstition Hill, *SJV*—San Jacinto Valley, and *TE*—Temecula Elsinore

seismicity parameters vary, we have divided the CFM faults into five groups (Table 1). The first and second groups are defined based on the slip rate. The first group of high slip-rate faults has segments with fast slip rates ( $\geq 6$  mm/year) such as the San Andreas and San Jacinto faults. The second group of low slip-rate faults has slip rates of  $< 6$  mm/year. The separation slip-rate of 6 mm/year is chosen somewhat arbitrarily. The third group consists of fault segments with aftershocks and includes aftershock sequences during the time period covered by the catalog (1981–2005). There are 15 aftershock defined fault segments which accommodated some of the large aftershock sequences such as the 1986 Palm Springs, 1987 Superstition Hill, 1990 Upland, 1992 Landers, 1994 Northridge, and 1999 Hector Mine.

The fourth group, which we call “defined by seismicity group,” consists of 5% of the CFM fault segments, which are defined mostly by using

seismicity. These seismicity distributions often exhibit swarm-like behavior. The seismicity clusters in the regions where these faults are defined form linear trends, which suggest the presence of fault segments. The separation of the seismicity defined segments from the other groups of CFM segments avoids the possible circular reasoning of inferring relationships between seismicity and faults that are defined based on seismicity. Only three of these segments have assigned slip-rates. The fifth group, which is called “unconstrained seismicity group,” consists of segments located near the edges or outside the SCSN monitoring region, which is about 20% of the CFM fault segments. The hypocenters near these segments are not well constrained and thus may exhibit unexpected biases.

Several segments that are difficult to categorize and could be in either the aftershock or seismicity defined groups were assigned to the aftershock group.

Table 1  
*Subdividing the SCEC/CFM Fault segments into Groups*

Fault type	Count	Count in %	Count with slip rate
Fast fault slip rate ( $\geq 6$ mm/year)	13	8	13
Slow fault slip rate ( $< 6$ mm/year)	95	58	39
Had main-shock rupture and aftershocks in the last 25 years	15	9	10
Defined mostly by seismicity	8	5	3
Seismicity distribution unconstrained	32	20	10
Total	162	100	75

Also, two high slip rate segments, the Parkfield segment of the San Andreas fault and the Brawley seismic zone are unusual because although they both have high slip rates of 34 and 20 mm/year, respectively, neither was assigned to the high slip-rate group. The Parkfield segment is outside the monitoring region of the SCSN and also had a  $M$  6 main shock-aftershock sequence in 2004. It was assigned to the unconstrained seismicity group. The Brawley seismic zone has a high slip rate however its geometrical shape is mostly based on seismicity. It was assigned to the defined-by-seismicity group. We also calculated the  $a$ -value and  $b$ -value Gutenberg–Richter parameters for each of the fault groups using the *zmap* software (WIEMER, 2001).

### 3. Results

Spatially clustered distributions of seismicity exist near the PSZs of all late Quaternary faults in southern California. We call these regions of small slip surfaces where these distributions are located seismic damage zones. These zones extend from the PSZs out to horizontal distances of  $\pm 10$  km. Most of the seismic damage zones are complex and the seismicity does not cluster at the PSZs, except for aftershocks. Instead, the PSZs are often illuminated by changes in the depth distributions of seismicity, with different depth distributions of seismicity on each side of the fault. In addition, often the rate of seismicity can be higher on one side than the other of the PSZs. These patterns of seismicity suggest that the PSZs are acting more as material discontinuities than zones of weakness where background seismicity is preferentially accommodated.

#### 3.1. Seismicity Patterns Near Selected PSZs

We have analyzed the interseismic seismicity of the three high slip-rate strike-slip faults (San Andreas, San Jacinto and Elsinore faults). We have also analyzed the pre-seismicity as well as the aftershock patterns of the 1992 Landers earthquake to illustrate the complex relationships between the seismicity and the PSZs.

##### 3.1.1 Southern San Andreas Fault

The cross-section histograms and the fault normal depth sections for the San Andreas segments illustrate the complex seismicity distributions in the immediate vicinity of the PSZs (Fig. 3). The central segments exhibit lower rates of background seismicity than the south segments. In general, the Chalome, Carrizo, Mojave, and San Bernardino segments exhibit a somewhat peaked level of activity within  $\pm 4$  km distance of the PSZs, and more distributed activity on the west side. They also exhibit different depth distributions on either side of the PSZs.

In the south, the damage zone seismicity is distributed over  $\pm 10$ -km-wide zones and the shapes of the histograms are very complex. The Banning, Mill Creek, Garnet Hill, and Coachella segments show distributions with the predominant activity on the east side of the PSZs. The complexity in the seismicity distribution is in part related to the multiple strands of the San Andreas fault through Banning and San Gregonio Pass.

Several segments, such as the Carrizo, Mojave, San Bernardino, and Mill Creek segments show evidence of seismic quiescence with a small decrease in the histogram values near the PSZs,

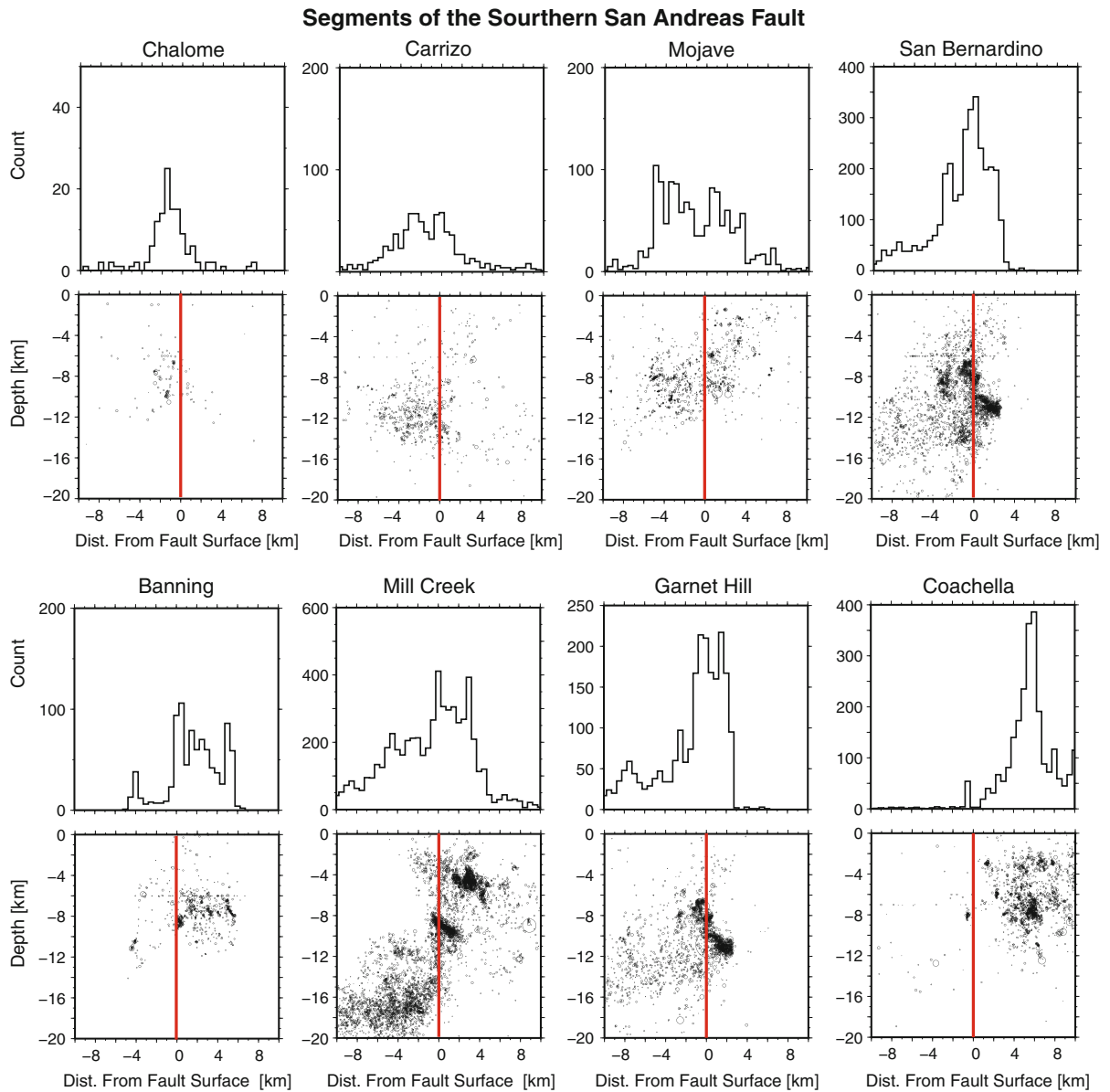


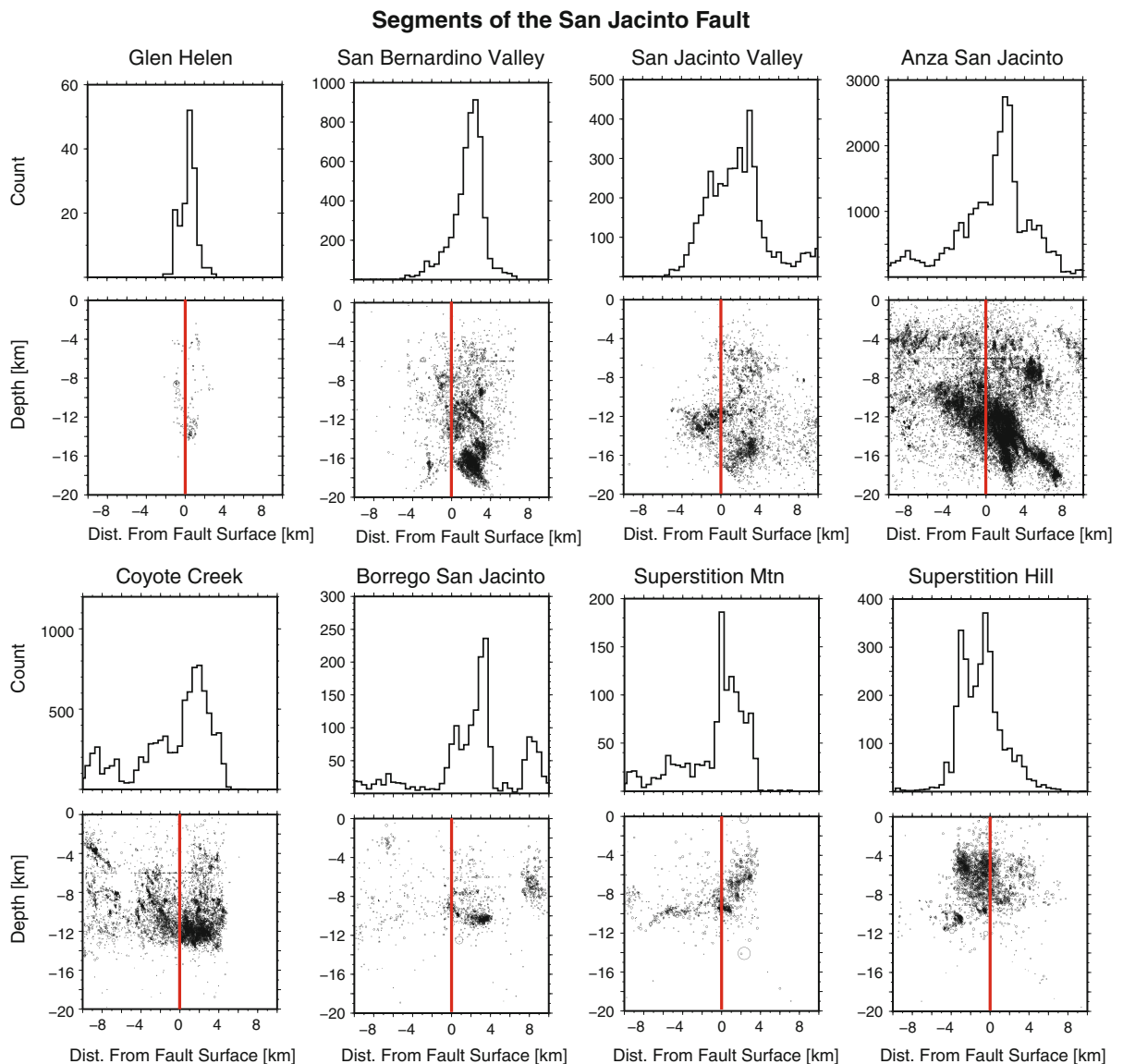
Figure 3

Histograms and depth sections for seismicity along segments of the San Andreas fault. The zero distance (*vertical reference line*) in depth sections is relative to the CFM surface and is the PSZ. The “Distance from CFM fault surface” is measured between each hypocenter and the nearest CFM triangular element of a fault surface. Thus, the PSZs for dipping faults are also vertical

although this decrease is probably not statistically significant. The presence of seismic quiescence near the core of the PSZs could indicate the possible presence of a very thin, almost not resolvable, zone of weakness or that the entire PSZ is locked and not slipping.

### 3.1.2 San Jacinto Fault

The San Jacinto fault zone exhibits the highest level of damage zone seismicity when compared to all other faults in southern California (Fig. 4). The corresponding depth distributions of the seismicity



Histograms and depth sections for seismicity along segments of the San Jacinto fault. The zero distance (*vertical reference line*) in depth sections is relative to the CFM surface and is the PSZ

also illustrate complex distributions and the absence of clustering near the PSZs. Often the density and depth distribution patterns are different on either side of the PSZs. The histograms of hypocentral distances for the San Jacinto fault segments exhibit different shapes and other complexity in part caused by their *en-echelon* juxtaposition with other CFM segments. In several cases this seismicity is clustered in

extensional step-overs, between the *en-echelon* fault segments. The north segments have distinct peaked distributions that are offset from the PSZs. In some cases the dip of the PSZ may not be correct and thus the seismicity is artificially offset. One of these segments, the seismic damage zone of the Anza San Jacinto segment differs from other damage zones because it has a considerably higher rate of seismicity

than adjacent segments. It also has a wide damage zone with three to five times the productivity associated with it when compared to the adjacent segments.

The southern segments, Coyote Creek, Borrego San Jacinto, Superstition Mountain, and Superstition Hill all exhibit changes in density of seismicity across the PSZs, with some of the seismicity clustered near the brittle-ductile transition zone. They all exhibit 4–6 km shallower seismicity than observed to the north (Fig. 4). The shallower seismicity is consistent with higher heat flow in this region.

### 3.1.3 *Elsinore Fault*

The seismicity distributions next to the PSZs of the Elsinore fault segments are diffuse (Fig. 5). The seismic damage zones around the north Elsinore PSZs exhibit similar seismicity rates as the San Andreas fault segments. The Whittier, Chino, Glen Ivy, and Temecula Elsinore segments exhibit low level of activity, with different seismicity rates on each side of the PSZs.

The Julian, Earthquake Valley, Coyote Mountain, and Laguna Salada segments have higher levels of seismicity, although the maximum depth of the seismicity becomes shallower to the south. Similar to some of the PSZs of the San Andreas fault, the Earthquake Valley segment apparently exhibits seismic quiescence around the PSZ in the depth range of 4–12 km. However, this could be an artifact because the PSZ associated seismicity and focal mechanisms suggest that it changes dip along strike (C. Nicholson, written communication, 2008). The seismic damage zones of the Chino and Earthquake Valley segments form asymmetric truncated distributions because the seismicity is assigned to other adjacent segments. The Julian and Coyote Mountain segments exhibit somewhat peaked histogram distributions near the PSZs. The corresponding depth distributions show no obvious features related to the PSZs except for the absence of shallow seismicity in the Coyote Mountain section as well as a higher seismicity rate on the east side. Thus, the Whittier, Chino, Temecula, and Laguna Salada PSZs are juxtaposing two crustal

blocks with different background seismicity rates. Although the Laguna Salada segment to the south has poorly defined seismicity, it shows a clear increase in seismicity from east to west.

### 3.1.4 *The 1992 Landers Sequence*

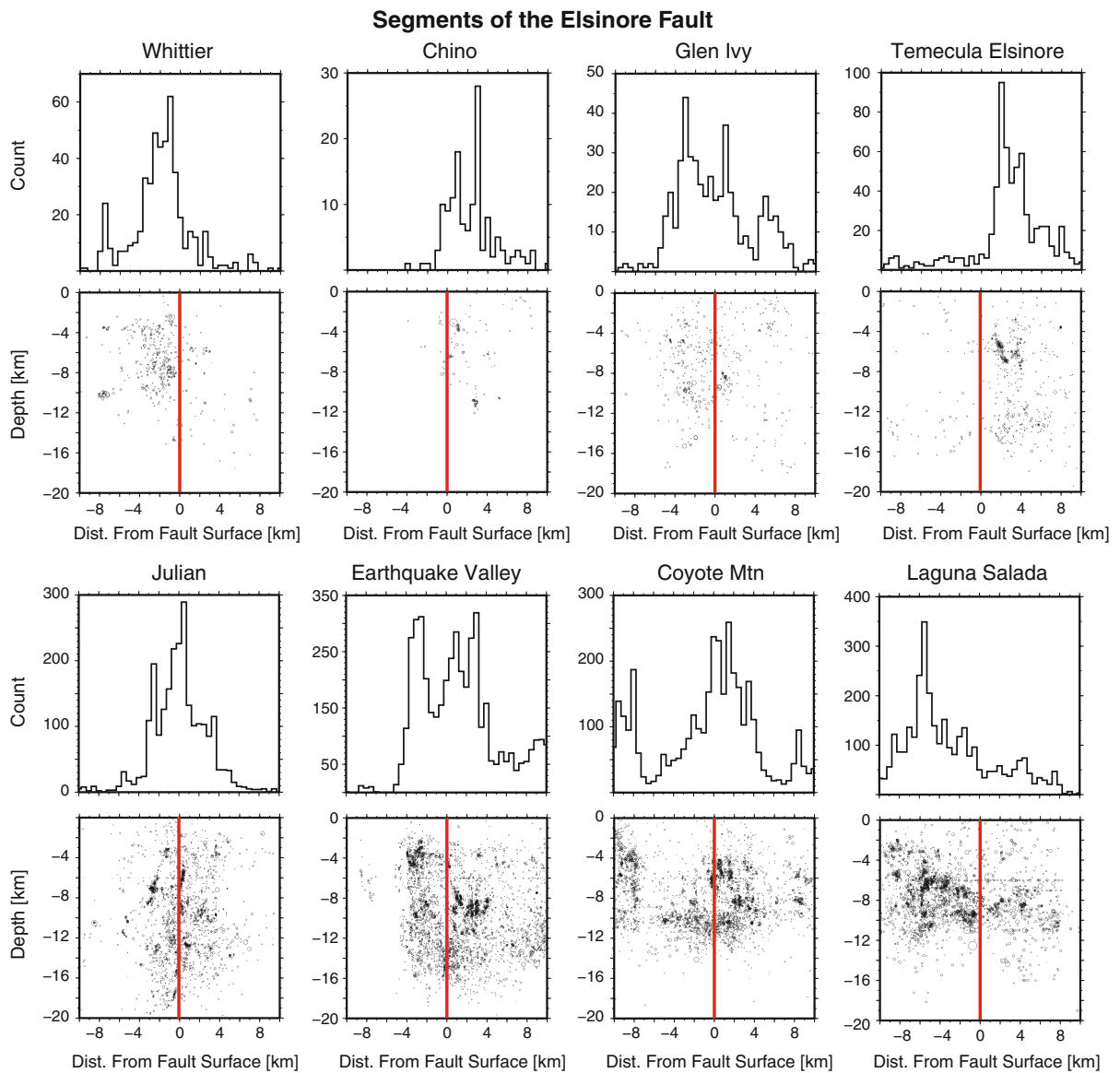
The fault-normal depth distributions of the 1992  $M_w$ 7.3 Landers seismicity recorded before and after the main shock are very different (Fig. 6). The 1981–1991 background seismicity preceding the main shock is a factor of 30 lower even though we combine the seismicity for all the Landers PSZs. It is distributed around the fault out to distances of  $\pm 10$  km as we observe for the other strike-slip faults. In contrast, the aftershocks around all of the Landers PSZs show peaked distributions with a kurtosis of  $\sim 10$ , which is larger than the kurtosis of  $\sim 0$  for the pre-main-shock background seismicity. The aftershock distributions are clearly centered on the PSZ, with an average width of  $\pm 2$  km.

The Johnson Valley, Homestead Valley, or Eureka Peak faults display peaked distributions with similar shapes. However, in some of the histograms and depth sections the seismicity is truncated by nearby fault segments, making artificial abrupt terminations to the distributions. The northernmost Camp rock segment, where the mainshock fault rupture terminated, has the lowest level of activity. Overall the aftershock depth distributions are symmetric, exhibit the highest level of seismicity at the PSZs, and decay with distance away from the PSZs.

### 3.1.5 *Summary*

The background seismicity and aftershocks form very different spatial patterns. The background seismicity appears to be driven by localized heterogeneous crustal shear and the availability of small slip surfaces near the PSZs. The density of these small slip surfaces decreases with distance away from the PSZs. In contrast, the aftershocks are clearly centered at the PSZ of the main shock, and probably driven by the heterogeneous stress field left behind by the main shock.





Histograms and depth sections for seismicity along segments of the Elsinore fault. The zero distance (*vertical reference line*) in depth sections is relative to the CFM surface and is the PSZ

### 3.2. Decay of Seismicity with Distance Away from PSZs

To explore the spatial relationship between the seismicity and the PSZs we have determined the distance decay of the fault normal density of seismicity. To search for possible differences in distance decay, we analyzed the decay rate of

interseismic background seismicity near high sliprate strike-slip faults, and the 1992 Landers aftershocks. We also compared the distance decay of the five groups of PSZs.

The fault normal density of the interseismic seismicity, next to three major strike-slip faults, shows a constant rate of seismicity within a  $\pm 2.5$ -km-wide

### 1992 Mw7.3 Landers Sequence

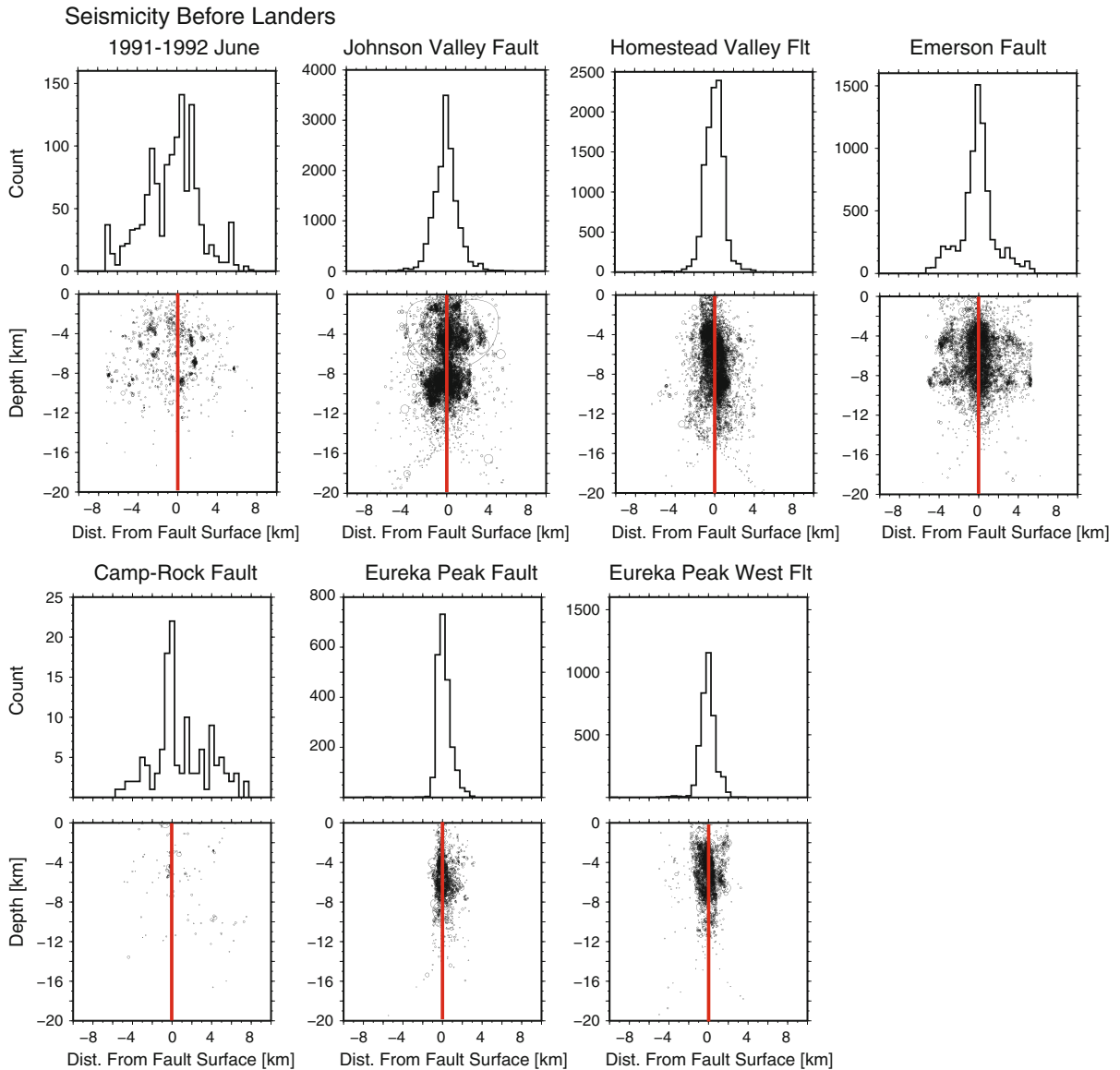


Figure 6

Histograms and depth sections for seismicity along segments that ruptured in the 1992 Landers sequence. The zero distance (*vertical reference line*) in depth sections is relative to the CFM surface and is the PSZ

fault zone (Fig. 7). The presence of the fault zone is consistent with geological features that form adjacent to major PSZs. Outside of the fault zone, the background seismicity rate decays at a rate ranging from  $10^{-1.28}$  to  $10^{-1.79}$ . The distance decay of seismicity could reflect a possible decrease in permeability and porosity, which affect effective strength, or

levels of tectonic stress as well as a decrease in availability of small slip surfaces.

The PSZs of the 1992 Landers earthquake exhibit similar constant rate of activity within a  $\pm 2$ -km-wide fault zone. Outside of the fault zone, the distance decay of pre-seismicity and aftershocks associated with the 1992 Landers surface rupture exhibits a

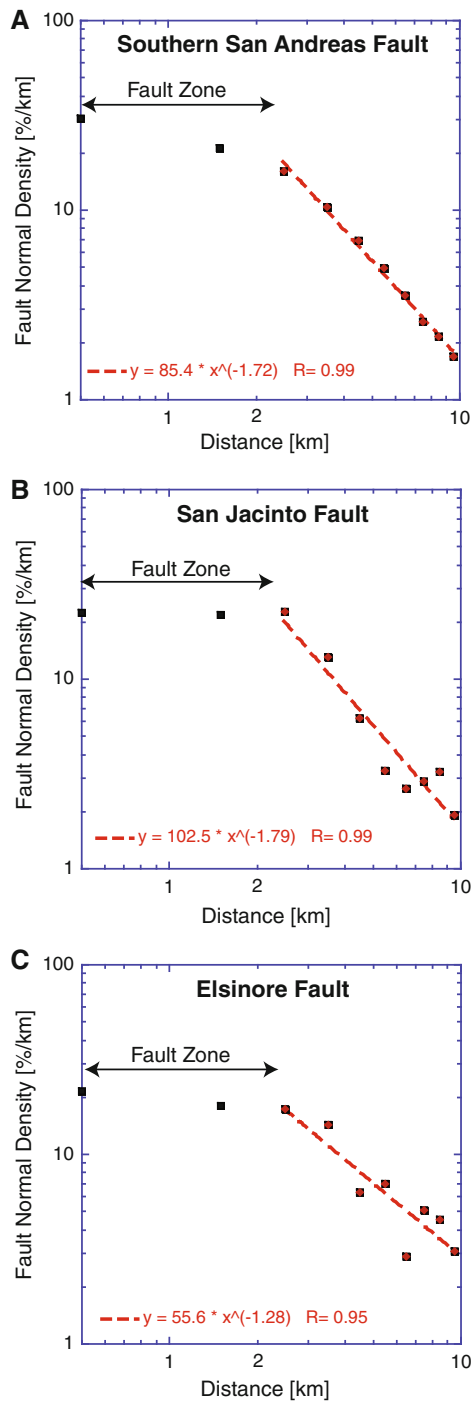


Figure 7

Decay of seismicity with distance for three high slip-rate faults, **a** San Andreas fault, **b** San Jacinto fault, and **c** Elsinore fault

sharp fall-off (Fig. 8). The preseismicity decay rate of  $10^{-2.0}$  is somewhat larger than what we observed for major strike-slip faults during their interseismic

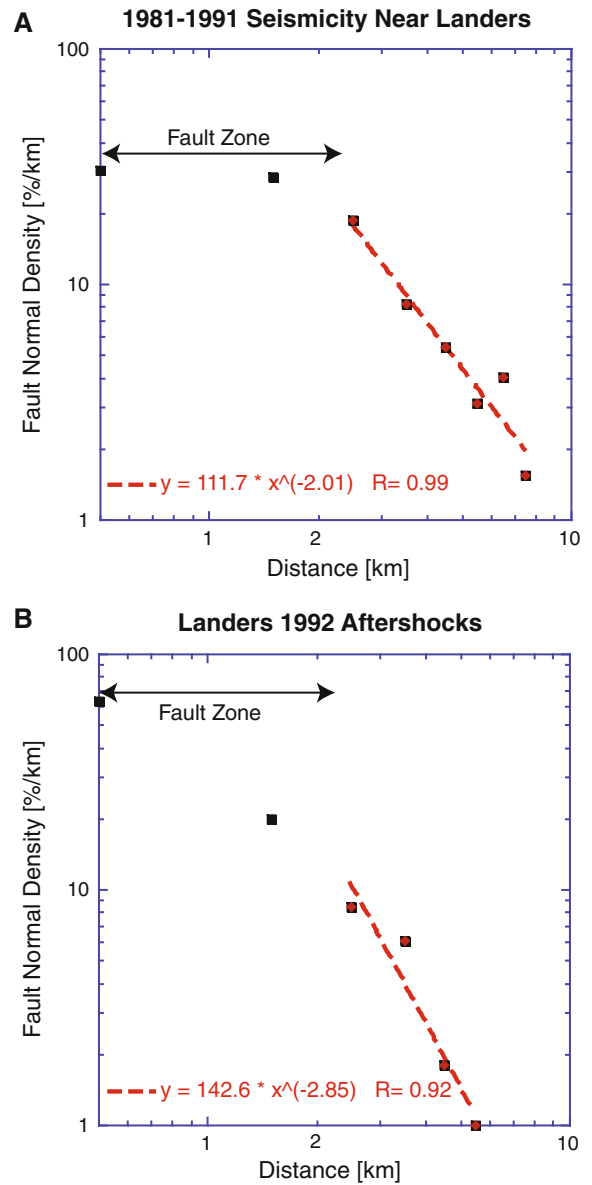


Figure 8

Decay of Landers seismicity with distance from the PSZs. **a** Distance decay of pre-main-shock seismicity; **b** Distance decay of aftershocks

period. The 1992 Landers aftershocks decay much faster with distance or as  $10^{-2.8}$ . The exponent of the power-law decay with distance for the 1992 Landers aftershocks is about twice as large as reported for smaller earthquakes (FELZER and BRODSKY, 2006). This difference may in part be explained because FELZER and BRODSKY (2006) analyzed a very selected data set. They analyzed all available main shocks in

selected magnitude ranges, as well as shorter time and larger spatial scales, which would have included both sequences close to and distant from PSZs.

The decay of seismicity with distance away from the PSZs appears to be a stationary feature of the seismicity. However, the aftershocks decay faster with distance than the interseismic seismicity

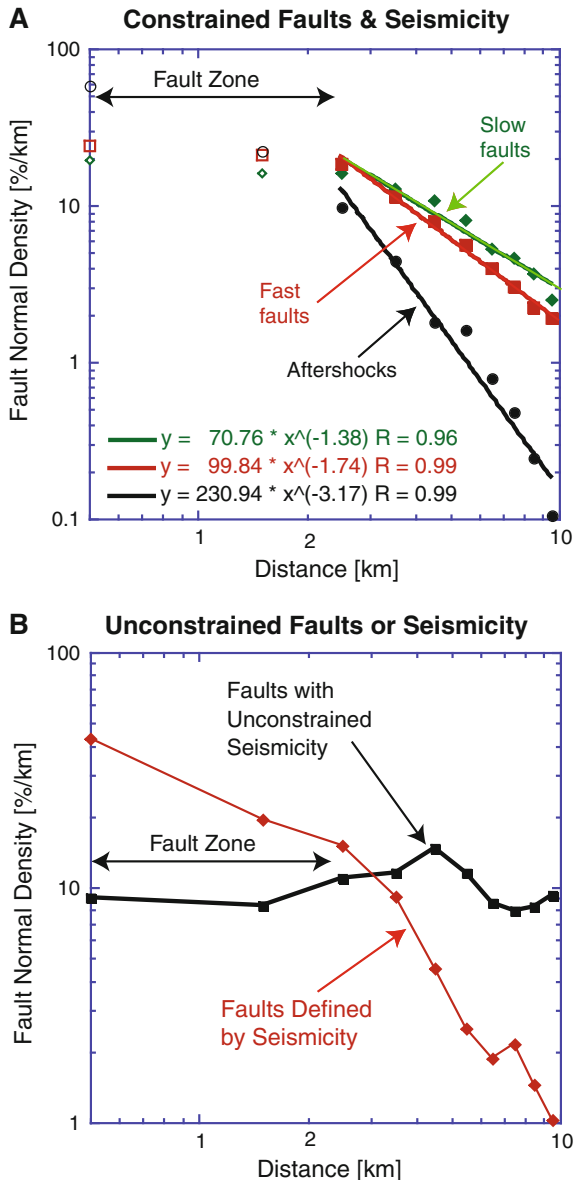


Figure 9

Fault normal density of hypocenters per kilometer plotted versus distance for the different groups of PSZs. **a** High slip-rate, low slip-rate, and aftershock groups; **b** Faults defined only by seismicity, and faults in which the seismicity in the region is not constrained caused by lack of seismic network coverage

adjacent to high and low slip rate faults (Fig. 9a). The high rate of decay of the aftershocks is consistent with the transient nature of aftershocks and non-elastic fracturing of the region surrounding the PSZs of the main shock. The similar distance decay rates for high and low slip-rate faults suggest that the geological moment rate does not affect the decay rate significantly.

The fourth and fifth fault groups that are defined by “seismicity” and by “unconstrained seismicity” exhibit complex distance decay (Fig. 9b). In particular for the group of faults with unconstrained seismicity, the distance decay is not present, reflecting the lack of constraints on the seismicity and possible incorrect association between seismicity and the PSZs. The group of faults that are defined by seismicity decays more irregularly than aftershock zones, in part because they are small data sets of earthquake swarms that exhibit behavior that is in between the behavior of background seismicity and aftershocks.

The distance decay patterns show that each PSZ is surrounded by an approximately  $\pm 2$ -km-wide weak zone with a constant rate of seismicity. At greater distances, to about 10 km, the seismicity decays to a low background level. Thus, a core fault zone surrounds the PSZs and accommodates the aftershocks and some fraction of the background seismicity. A damage zone containing mostly small slip surfaces and gradually decaying with distance, accommodates elevated seismicity to  $\sim 10$  km distance. One of many possible explanations for the presence of the damage zone is a wide zone of strain softening surrounding the PSZs. Alternatively, continuous slip below the brittle-ductile transition could load the slip surfaces of small earthquakes within the damage zone, resulting in elevated background seismicity.

### 3.3. Seismicity Characteristics Associated with each Fault Group

We have compared the seismicity parameters with the geological parameters of the PSZs (Fig. 10). The geological parameters describing each PSZ are the slip-rate and the geologic moment rate. The ‘slip-rate’ multiplied by ‘fault area’ is equivalent to geologic moment rate, and thus can be considered a

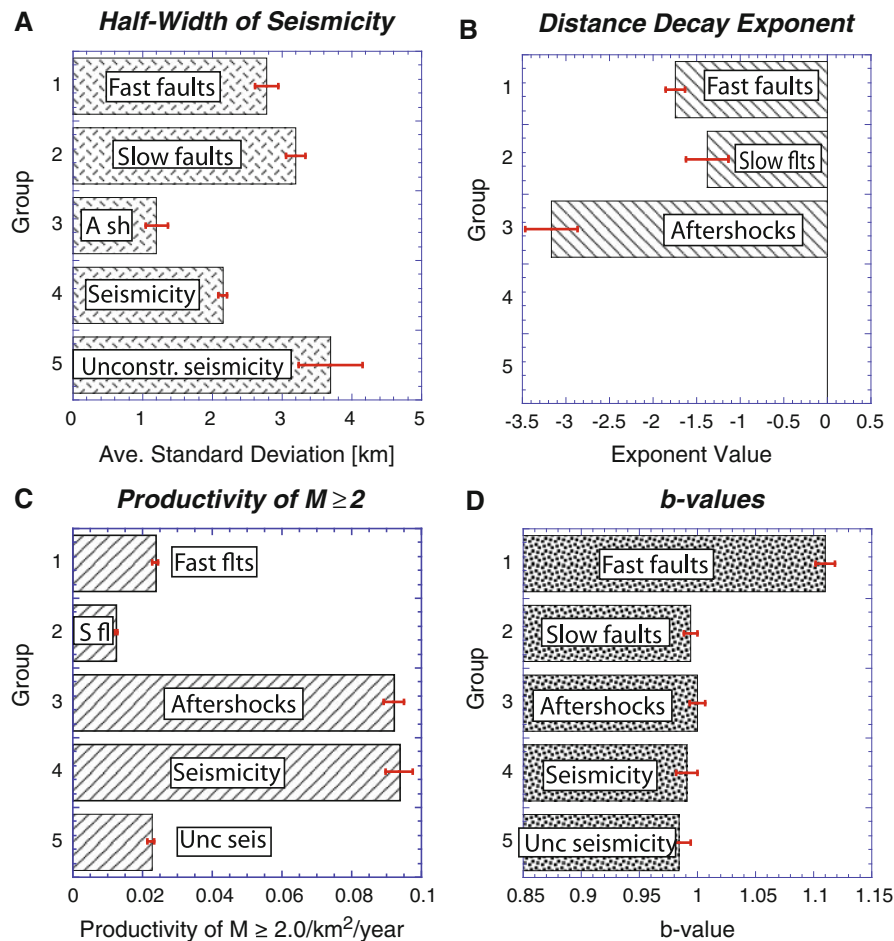


Figure 10

Bar graphs of seismicity parameters for the five fault groups of PSZs. The PSZs are divided into five groups as discussed in the text. *Error bars* of  $\pm 1\sigma$  are included. **a** Half-width of the histogram distributions of hypocentral distances; the “half-width” is calculated as the statistical “average deviation” or the statistical width of each histogram; “A sh”—aftershock fault group. **b** Distance decay parameter; this parameter is not available for PSZs that are defined by seismicity or are located near the edges or outside the network reporting area; **c** Seismicity productivity of  $M \geq 2.0$  per area and year for each of the groups; “s fl”—slow faults group, “Unc seis” unconstrained seismicity fault group; and **d**  $b$ -value for each of the groups. “Unc seismicity” unconstrained seismicity fault group

proxy for the long-term tectonic strain loading along a particular CFM fault segment.

The seismicity parameters of each of the five PSZ groups are the standard deviation (the halfwidth of each seismicity distribution clustered around the PSZs), the distance decay, the productivity [derived from the  $a$ -value as  $(10^{*(a\text{-value} - 2.0*b\text{-value})}/\text{area})$ ] and  $b$ -value, which quantifies the relative rate of large and small earthquakes. The productivity is the rate of  $M \geq 2$  events per area and per year. Other geometrical distribution parameters such as skewness and kurtosis are not easily interpreted and do not exhibit simple relationships with the parameters of

the PSZs. The uncertainty in the half-width of seismicity was determined by calculating the difference in the half-width for the full data set and half the data set. Similarly, the uncertainty in the distance decay exponent was determined by removing one data value from the regression calculation at a time. The  $b$ -value uncertainty estimate is approximately  $b/\sqrt{N}$  for large  $N$  where  $N$  is the number of earthquakes with magnitude larger than the magnitude of completeness (UTSU, 2003). The productivity uncertainty was determined from the  $b$ -value uncertainty by estimating the change in productivity from the minimum and maximum  $b$ -value slopes.

The seismicity distributions for the five different fault groups have different half-widths and range from 1 km for aftershocks to  $\sim 4$  km for unconstrained seismicity (Fig. 10a). The aftershock-defined and seismicity-defined faults have the narrowest distributions. The fast and slow slip-rate faults along with unconstrained seismicity faults have the broadest distributions. The distance decay rate is more rapid for aftershock-defined faults than for fast and slow slip-rate faults with interseismic seismicity (Fig. 10b). Thus aftershocks, and the interseismic background seismicity behave differently. This difference in behavior could be interpreted as being caused by the heterogeneous strain-field in the immediate vicinity of the PSZs which was left behind by the main shock.

The productivity is considerably higher for the aftershock-defined and seismicity-defined fault groups (Fig. 10c). The fast slip-rate, slow slip-rate, and unconstrained seismicity faults have lower productivity. In part, this result is expected because aftershock sequences are much more productive and constitute more than half of the southern California earthquake catalog. As a group, the high slip-rate faults exhibit the largest  $b$ -value (Fig. 10d). The low productivity and high  $b$ -value of high slip-rate faults is in agreement with the absence of moderate-sized events within their seismic zones. In particular, there is a lack of main shock-aftershock sequences in the intermediate magnitude range from  $M$  5 to  $M$  7.

There is an inverse relationship between the half-width of the fault groups and their productivity (Fig. 11). The aftershock-defined and seismicity-defined segments have very narrow and high producing distributions. The other three groups of faults that are in essence in their interseismic period have broader distributions with lower productivity. This observation is consistent with the main-shock rupture providing most of the heterogeneous driving strain field for the aftershocks. During the interseismic period all the faults seem to behave similarly.

The characteristic time and space clustering features of aftershock distributions suggest that the background seismicity within the  $\pm 10$ -km-wide seismic damage zone is not aftershocks, and is not accommodating seismic slip on the corresponding PSZ. Because the aftershock distributions do not

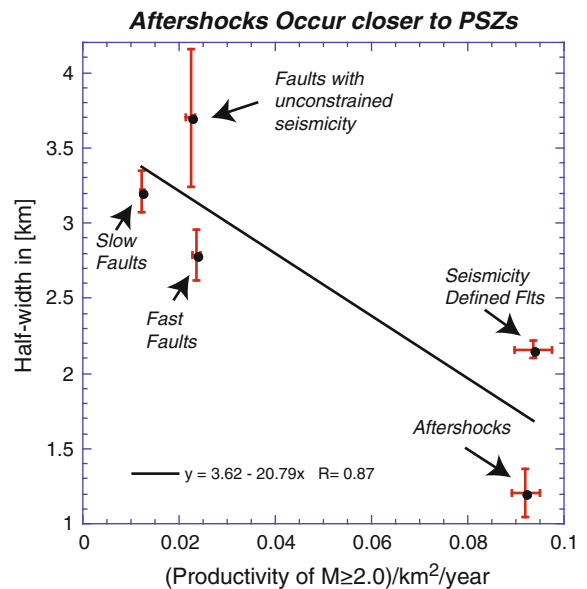


Figure 11

Half-width of seismicity distributions plotted versus productivity. Data points representing the five fault groups (Table 1) are labeled. Error bars of  $\pm 1\sigma$  are included. On average, the aftershock segments and the seismicity defined segments are narrower and exhibit higher productivity than faults in the interseismic stage

diffuse away from the PSZs and maintain their initial spatial distribution (HELMSTETTER *et al.*, 2003), it is easy to compare their spatial patterns to the background seismicity. Using the halfwidth versus productivity relations, we can separate the aftershock distributions from the background seismicity distributions. These results for aftershocks are consistent with the clustering models of ZALIAPIN *et al.* (2007) who showed that aftershocks form a statistically distinct clustered spatial group from background seismicity.

The high slip-rate faults are the most important faults because they are responsible for most of the earthquake hazards. The slip-rate by itself gives instantaneous deformation rate while the slip-rate multiplied by fault area is a proxy for the long-term strain release rate. For the high slip-rate faults, both the productivity and  $b$ -value show variations with slip-rate and geologic moment rate (Fig. 12). The uncertainties in geological slip rates are from FRANKEL *et al.* (2002). The three most productive fault segments in southern California are the Anza San Jacinto segment, Imperial fault, and the San Andreas Mill Creek fault segment. The high

productivity of the first two fault segments includes seismicity along the whole length of the faults. The Mill Creek segment of the San Andreas fault that includes a number of earthquakes at depth below Banning Pass is not an obvious high seismicity producer. In contrast, the three segments of the San Andreas fault: Chalome, Carrizo, and Mojave, exhibit extremely low productivity which can be attributed both to large cumulative offset and associated smoothing.

In Figs. 12c, d, the  $b$ -value plots display no clear trends, although the SAF segments to the north tend to have  $b$ -values on the high side. Small events are less common within the SAF damage zones, and some of the heterogeneity within the seismic damage

zone could have been removed through high cumulative offset. The combined high  $b$ -value and low productivity for the SAF segments are in agreement with the observed absence of moderate-sized events adjacent to these faults.

#### 4. Discussion

The clusters of background seismicity near the PSZs may be related to the cumulative offset or slip-rate of the faults. If some faults were older with large cumulative offset or weaker than others, we would expect that the corresponding seismicity distributions

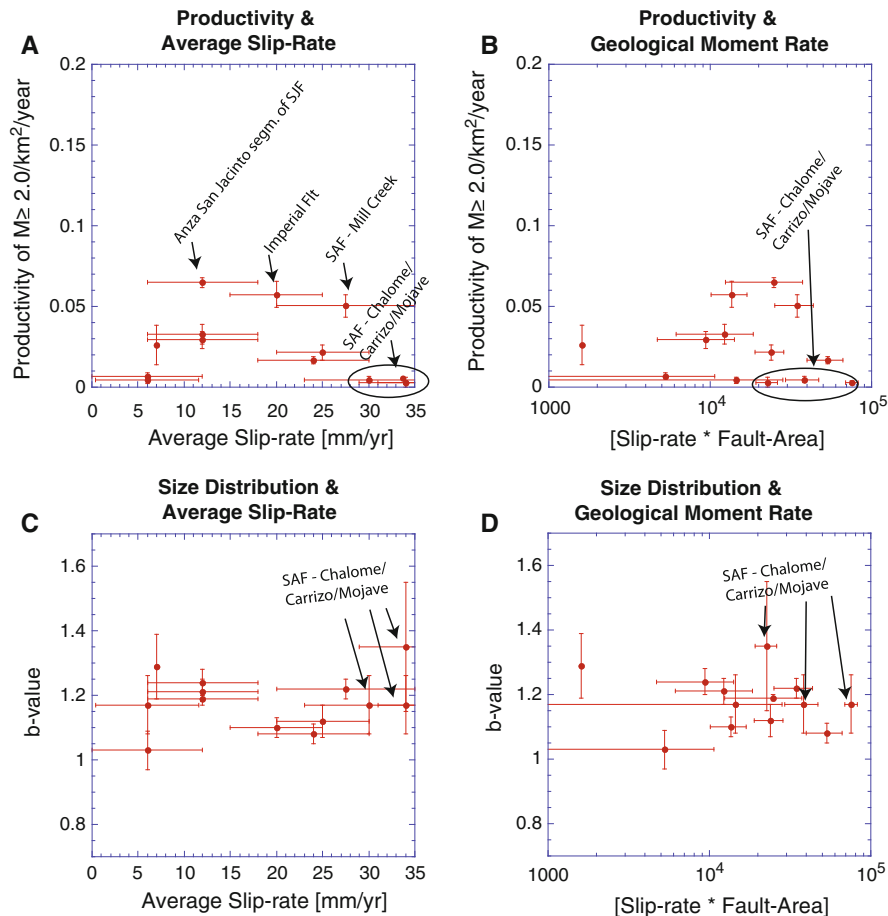


Figure 12

Comparison of fault parameters and seismicity parameters for high slip-rate fault segments. *Error bars* of  $\pm 1\sigma$  are included. **a**, **b** show productivity and  $b$ -value versus average sliprate. Productivity is the rate of  $M \geq 2.0$  events normalized per area and per year. High productivity and San Andreas fault segments are labeled. **c** shows productivity normalized by area and year, and **d** shows  $b$ -value versus geologic moment rate that is represented by (Slip\* Fault Area). San Andreas fault segments that exhibit low productivity and high  $b$ -values are also labeled

could have different geometrical shapes or degree of clustering. For instance, the San Andreas fault is old and if its PSZs were exceptionally weak, we would expect that the background seismicity could be concentrated within or close to the PSZs, similar to what is observed along the creeping section in central California (PROVOST and HOUSTON, 2001). We do not observe such clustering next to the PSZs of the southern San Andreas fault. Similarly, only the three fastest moving PSZs of the San Andreas fault (Chalome, Carrizo, and Mojave) have unusually low productivity. Thus, the nearfault background seismicity appears to be mostly controlled by factors other than cumulative offset or slip-rate.

One possible explanation for the seismic damage zones is that they form as part of the fault to accommodate bends and other geometrical irregularities (Fig. 13). As the fault accumulates more offset, beyond its initial formation, the widths of the inner  $\pm 2$ -km-wide fault zone and the outer seismic damage zone do not change significantly. However, the rate of background seismicity within the seismic damage zone, or seismic productivity, may remain high during the initial offset and associated smoothing of the secondary heterogeneous fault networks. In particular, the seismic damage zone of the Anza San Jacinto segment of the San Jacinto fault

accommodates a considerably higher level of seismicity than any other fault segments.

The productivity of a seismicity distribution may also depend on where within the seismic cycle the fault segment happens to be. If the fault just had a main shock, the seismic damage zone may be dominated by aftershocks such as the 1992 Landers PSZs. If the fault is late in the seismic cycle, it may be in a state of seismic quiescence. Similarly, external effects such as triggering by nearby main shocks or regional stress release caused by other earthquakes may influence the seismicity.

The relative strength of faults and the crust play an important role in understanding crustal strength (HARDEBECK and MICHAEL, 2006). The strength of faults is often presumed to vary with slip-rate, because fast moving faults slip a longer distance and more quickly remove geometrical irregularities and become weaker. Also, fast moving faults may be weaker because they have less time to heal. The features of damage zone seismicity thus may reflect some combination of the overall crustal strength in the region rather than the strength or slip-rates of individual faults. HARDEBECK and MICHAEL (2006) proposed a model of “*all major active faults being weak*” which explains our results of lack of special seismicity features for high slip-rate faults. The properties of the seismic damage zones of the San Andreas and San Jacinto faults are very similar to the other faults, suggesting similar fault strength.

The damage zone seismicity can also be affected by the crustal structure and heat flow as modeled by BEN-ZION and LYAKHOVSKY (2006). The more complex histograms that are observed to the south as compared to the north along the San Andreas, San Jacinto, and Elsinore faults suggest a different explanation for the seismicity than the influence of the PSZs. The tectonic difference between the northern and southern parts of our study region is the presence of the extensional tectonics and high heat flow to the southeast. The damage zones of fault segments located to the north of the Salton Trough and in areas of low to moderate heat flow, have a lower rate of seismicity and are spatially concentrated along only a few PSZs. The damage zones of fault segments located in the higher heat flow areas of the Salton Trough have a shallower brittle-ductile

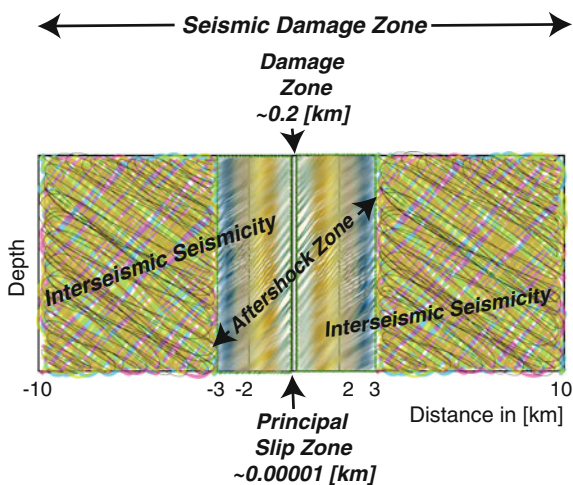


Figure 13

Cartoon cross section of fault structure illustrating the very narrow ( $\sim 1$  to  $10$  mm) PSZ, the  $\sim 200$ -m-wide damage zone determined from field mapping, and the  $\sim 10$ -km-wide seismic damage zone



transition (NAZARETH and HAUSSON, 2004). They are also more numerous and have higher seismicity rates, although their width remains overall very similar as observed in other parts of southern California. This suggests that the seismic damage zones are of similar width but less productive where the seismogenic zone is thick.

The intensity of aftershocks along the PSZs could be caused by coseismic stress variability (MARSAN, 2006). Smooth static stress models predict a seismicity shadow along the aftershock zone because the main shock released most of the available shear stress. MARSAN (2006) suggested that the onset of the seismicity shadow is delayed following the main shock. We observe such seismicity shadows along some of the fault segments that are in the interseismic period such as the low productivity segments of the southern San Andreas fault and the Earthquake Valley segment of the Elsinore fault. Thus these segments may have released all the stress heterogeneity associated with the last main shock.

We have also compared our results with theoretical rupture models of SHAW (2004) who proposed that event sizes scaled with segment length. Similarly, SHAW (2006) showed preferential epicenter clustering of small events at the end of the major fault segments in his model. We do not detect similar behavior of seismicity near late Quaternary faults in southern California. There are no obvious concentrations of events near segment ends and seismicity rates do not simply scale with fault length.

Previous studies have attempted to relate the seismicity rate with cumulative fault offset. WESNOUSKY (1990) inferred that seismicity rate adjacent to late Quaternary faults in southern California is controlled by cumulative fault offset. His Figs. 4 and 5 suggests that normalized productivity ( $a$ -value/areal slip-rate) decreases with cumulative offset. We see only minor hints of this effect when we plot productivity versus slip-rate, which is a proxy for cumulative offset. The normalization by area is the correct procedure but because area has high variability, it tends to dominate the small variations in the  $a$ -value. We obtain a slope of  $\sim 1.09$ , which suggests at most a 9% effect on the scaling of  $a$ -value with cumulative offset, which is significantly smaller than that which WESNOUSKY (1990) implied.

It is beyond the goals of this study to thoroughly analyze the scaling relations between the different populations of events that occur within fault zones. The background seismicity manifests self-similar scaling when major events along the PSZs are not included. The PSZs may evolve with time and interact with the background seismicity. ANDO and YAMASHITA (2007) suggested that the self-similar scaling between small and large earthquakes breaks down because the major earthquakes can form fault branches through strong nonlinear interactions.

Other studies have also discovered spatial and temporal heterogeneities in the crustal processes in southern California, which in part explains the heterogeneity in the seismicity distributions. SPOTILA *et al.* (2007) who modeled the long-term vertical crustal deformation around the San Andreas fault showed that fault convergence in the near-field of the fault does not completely accommodate oblique plate motion. They inferred that vertical deformation along the San Andreas fault was influenced by relative slip partitioning as well as other factors such as surface processes, crustal anisotropy, and strain-weakening. They pointed out that heterogeneous deformation may be maintained through a positive-feedback effect of strain-softening. WOESSNER and HAUSSON (2006) documented effects of strain-softening following the 1992 Landers earthquake. They found a small signal suggesting that the strain rate within the damage zones is higher the closer the seismicity is to the PSZs. The presence of the PSZs,  $\pm 2$ -km-wide fault zones, and the  $\pm 10$ -km-wide seismic damage zones also agrees with a mode of deformation that includes positive-feedback strain-softening.

## 5. Conclusions

The majority of small earthquakes do not occur on the same principal slip surfaces (PSZs) of late Quaternary faults in southern California as the major earthquakes. The background seismicity only exhibits weak clustering surrounding the different PSZs, forming  $\pm 10$ -km-wide seismic damage zones. In contrast, aftershocks are clustered around the PSZs and decay away both in time and space. The 3-D geometrical shapes and productivities of these zones

are similar, although they may be influenced by many factors, including the slip rates and the geological moment rates as well as the elapsed time since the last major earthquake on a PSZ. One possible interpretation is that the geometry of seismic damage zones develops early in the history of a fault, or alternatively the strengths of the near-fault crustal materials are very similar. For high slip-rate faults, the productivity of background seismicity of the damage zones is low in regions with thick crust. Because small and major earthquakes occur on spatially separated surfaces, their source physics may be different, with only large earthquakes being able to nucleate on the PSZs.

### Acknowledgments

This research was supported by the US Geological Survey Grant 08HQGR0030 to Caltech, and by the Southern California Earthquake Center. SCEC is funded by NSF Cooperative Agreement EAR-0529922 and USGS Cooperative Agreement 07HQAG0008. We thank L. Jones and P. Shearer for feedback and discussions; and PAGEOPH reviewers and editors for detailed comments. Most figures were done using GMT (WESSEL and SMITH 1998). We thank A. Plesch for doing the distance measurements. SCEC contribution number 1214. Contribution number 10,007, Seismological Laboratory, Division of Geological and Planetary Sciences, California Institute of Technology, Pasadena.

### REFERENCES

- ANDO, R. and YAMASHITA, T. (2007), *Effects of mesoscopic-scale fault structure on dynamic earthquake ruptures: Dynamic formation of geometrical complexity of earthquake faults*, J. Geophys. Res. *112*, B09303, doi:[10.1029/2006JB004612](https://doi.org/10.1029/2006JB004612).
- BEN-ZION, Y. and LYAKHOVSKY, V. (2006), *Analysis of aftershocks in a lithospheric model with seismogenic zone governed by damage rheology*, Geophys. J. Int. *165*, 197–210 doi: [10.1111/j.1365-246X.2006.02878.x](https://doi.org/10.1111/j.1365-246X.2006.02878.x).
- CHAMBON, G., SCHMITTBUHL, J., CORFDIR, A., ORELLANA, N., DIRAISON, M. and GÉRAUD, Y. (2006), *The thickness of faults: From laboratory experiments to field-scale observations*, Tectonophysics *426*, 77–94.
- FELZER, K.R. and BRODSKY, E.E. (2006), *Decay of aftershock density with distance indicates triggering by dynamic stress*, Nature *441*, 735–738.
- FRANKEL, A.D. *et al.* (2002), *Documentation for the 2002 Update of the National Seismic Hazard Maps*, Tech. Rep. Open-File Report 02-420, US Geological Survey.
- HARDEBECK, J.L. and MICHAEL, A. (2006), *Spatial and temporal stress inversion*, J. Geophys. Res. *111*, B11310, doi: [10.1029/2005JB004144](https://doi.org/10.1029/2005JB004144).
- HELMSTETTER, A., OULLON, G. and SORNETTE, D. (2003), *Are aftershocks of large California earthquakes diffusing?*, J. Geophys. Res. *108*, doi:[10.1029/2003JB002503](https://doi.org/10.1029/2003JB002503).
- JENNINGS, C.W. (1994), *Fault activity map of California and adjacent areas*: California Department of Conservation, Division of Mines and Geology, Geologic Data Map No. 6, scale 1:750,000.
- LIN, G., SHEARER, P.M. and HAUSSON, E. (2007), *Applying a three-dimensional velocity model, waveform cross correlation, and cluster analysis to locate southern California seismicity from 1981 to 2005*, J. Geophys. Res. *112*, B12309, doi:[10.1029/2007JB004986](https://doi.org/10.1029/2007JB004986).
- LIU, J., SIEH, K. and HAUSSON, E. (2003), *A structural interpretation of the aftershock “cloud” of the 1992  $M_w$ 7.3 Landers Earthquake*, Bull. Seismol. Soc. Am. *93*, 3, 1333–1344.
- MARSAN, D. (2006), *Can coseismic stress variability suppress seismicity shadows? Insights from a rate-and-state friction model*, J. Geophys. Res. *111*, B06305, doi:[10.1029/2005JB004060](https://doi.org/10.1029/2005JB004060).
- NAZARETH, J.J. and HAUSSON, E. (2004), *The seismogenic thickness of the southern California crust*, Bull. Seismol. Soc. Am. *94*, 940–960.
- PLESCH, A., SHAW, J.H., BENSON, C., BRYANT, W.A., CARENA, S., COOKE, M., DOLAN, J., FUIS, G., GATH, E., GRANT, L., HAUSSON, E., JORDAN, T., KAMERLING, M., LEGG, M., LINDVALL, S., MAGISTRALE, H., NICHOLSON, C., NIEMI, N., OSKIN, M., PERRY, S., PLANANSKY, G., ROCKWELL, T., SHEARER, P., SORLIEN, C., SÜSS, M.P., SUPPE, J., TREIMAN, J., and YEATS, R. (2007), *Community fault model (CFM) for southern California*, Bull. Seismol. Soc. Am., Dec., *97*, 1793–1802.
- PRESS, H.W., TEUKOLSKY, S.A., VETTERLING, W.T. and FLANNERY, B.P., *Numerical Recipes in Fortran 77, The Art of Scientific Computing*, 2nd Edition, Vol. 1 (Cambridge University Press, New York, NY (1997)) 1447 pp.
- PROVOST, A.-S. and HOUSTON, H. (2001), *Orientation of the stress field surrounding the creeping section of the San Andreas Fault: Evidence for a narrow mechanically weak fault zone*, J. Geophys. Res., *106*, B6, 11,373–11,386.
- SAGY, A., BRODSKY, E.E. and AXEN, G.J. (2007), *Evolution of fault-surface roughness with slip*, Geol. *35*, 283–286.
- SIEH, K., JONES, L.M., HAUSSON, E., HUDNUT, K., EBERHART-PHILLIPS, D., HEATON, T.H., HOUGH, S., HUTTON, K., KANAMORI, H., LILJE, A., LINDVALL, S., MCGILL, S.F., MORI, J., RUBIN, C., SPOTILLA, J.A., STOCK, J., THIO, H.K., TREIMAN, J., WERNICKE, B. and ZACHARIASEN, J. (1993), *Near-field investigations of the Landers earthquake sequence April–July 1992*, Science *260*, 171–175.
- SHAW, B.E. (2004), *Variation of large elastodynamic earthquakes on complex fault systems*, G. Res. Lett., *31*, L18609, doi:[10.1029/2004GL019943](https://doi.org/10.1029/2004GL019943).
- SHAW, B.E. (2006), *Initiation propagation and termination of elastodynamic ruptures associated with segmentation of faults and shaking hazard*, J. Geophys. Res. *111*, B08302, doi:[10.1029/2005JB004093](https://doi.org/10.1029/2005JB004093).
- SIBSON, R.H. (2003), *Thickness of the seismic slip zone*, Bull. Seism. Soc. Am. *93*, 3, 1169–1178; doi:[10.1785/0120020061](https://doi.org/10.1785/0120020061).

- SPOTILA, J., NIEMI, A., BRADY, R., HOUSE, M., BUSCHER, J. and OSKIN, M. (2007), *Long-term continental deformation associated with transpressive plate motion: The San Andreas fault*, *Geology* 35, 11, 967–970; doi:[10.1130/G23816A.1](https://doi.org/10.1130/G23816A.1);
- UTSU, T., *Statistical Features of Seismicity*, *Int'l. Handbook of Earthquake and Engineering Seismology V. 81B: Centennial publication of the Intl'. Assn. of Seism. and Physics of the Earth's Interior* (P. Jennings, H. Kanamori, and W. Lee, eds), pp. 719–732 (2003).
- WESNOUSKY, S.G. (1990), *Seismicity as a function of cumulative geologic offset: Some observations from southern California*, *Bull. Seism. Soc. Am.* 80, 1374–1381.
- WESSEL, P. and SMITH, W.H.F. (1998), *New version of the generic mapping tools released*, *EOS* 79, 579.
- WESSON, R.L., BAKUN, W.H. and PERKINS, D.M. (2003), *Association of earthquakes and faults in the San Francisco Bay Area using Bayesian inference*, *Bull. Seismol. Soc. Am.* 93, 1306–1322.
- WIEMER, S. (2001), *A software package to analyze seismicity: ZMAP*, *Seis. Res. Lett.*, 373–382.
- WOESSNER, J. and HAUKSSON, E. (2006), *Associating Southern California seismicity with Late Quaternary Faults: Implications for Seismicity Parameters (abstract)*, Southern California Earthquake Center Annual Meeting, Palm Springs, CA.
- WOOD, H.O. (1916), *The earthquake problem in the Western United States*, *Bull. Seismol. Soc. Am.* VI, 196–217.
- ZALIAPIN, I., GABRIELOV, A., KEILIS-BOROK, V. and WONG, H. (2007), *Aftershock identification*, *arXiv:0712.1303v1 [physics.geo-ph]*.

(Received August 5, 2008, revised March 11, 2009, accepted May 24, 2009, Published online March 18, 2010)